Electronic Supplementary Information

Redox-Active Metal-Organic Framework Mediator Enables Enhanced Polysulfide Confinement and Streamlined Reaction Pathways in Lithium-Sulfur Batteries

Qinghan Zeng ǂ [a], Ruishan Zhang ǂ [b], Haibin Lu[a], Junhua Yang[a], Jionghui Rong[a], Jingqia Weng[a], Bingkai Zhang[b], Shiyun Xiong[a], Qi Zhang*[ac], and Shaoming Huang*[ad]

[a] Guangzhou Key Laboratory of Low-Dimensional Materials and Energy Storage Devices, School of Materials and Energy, Guangdong University of Technology, Guangzhou, 510006, China. E-mail: qzhangmse@gdut.edu.cn; smhuang@gdut.edu.cn

[b] School of Chemical Engineering and Light Industry, Guangdong University of Technology, Guangzhou, 510006, China.

[c] State Key Laboratory of Silicon and Advanced Semiconductor Materials, Zhejiang University, Hangzhou, 310027, China.

[d] School of Chemistry and Materials Science, Hangzhou Institute for Advanced Study, University of Chinese Academy of Sciences, Hangzhou, 310024, China

ǂ These authors contributed equally to this work.

Experimental Procedures

Materials

Chromium nitrate nonahydrate ($Cr(NO_3)_3 \cdot 9H_2O$, 99.95%, Aladdin), DL-Dithiothreitol (DTT, 99%, Aladdin), terephthalic acid (H_2BDC, 99%, Sigma-Aldrich), acetylene black (Denka Black Li-2060, Hefei Saibo New Materials Co., Ltd), ketjenblack (KB, ECP-600JD, Canrd Technology Co. Ltd.), graphite oxide (GO, SE2430, The Sixth Element Materials Technology Co., Ltd), graphene (The Sixth Element Materials Technology Co., Ltd), hydrofluoric acid (40% Guangzhou Chemical Reagent Factory), N, N-dimethylformamide (DMF, 99.9%, Shanghai Aladdin Biochemical Technology Co., Ltd.), 1,3-dioxolane (DOL, Shanghai Aladdin Biochemical Technology Co., Ltd.), 1,2-dimethoxyethane (DME, Shanghai Aladdin Biochemical Technology Co., Ltd.), trichloromethane ($CHCl_3$, Shanghai Aladdin Biochemical Technology Co., Ltd.), polyvinylidene fluoride (PVDF, Shanghai Aladdin Biochemical Technology Co., Ltd.), sublimed sulfur (99.5%, Shanghai Aladdin Biochemical Technology Co., Ltd.), N-methyl pyrrolidone (NMP, 99.9%, Shanghai Aladdin Biochemical Technology Co., Ltd.), acetonitrile (99.5%, Shanghai Aladdin Biochemical Technology Co., Ltd.), tetraethylene glycol dimethyl ether (99.5%, Shanghai Aladdin Biochemical Technology Co., Ltd.) polyoxyethylene (PEO, Shanghai Aladdin Biochemical Technology Co., Ltd.). All chemical reagents were used as received without further processing.

Preparation of MIL-101(Cr)

$Cr(NO_3)_3 \cdot 9H_2O$ (800 mg, 2 mM) and terephthalic acid (332 mg, 2 mM) were dissolved in 14 mL of deionized water, supplemented with 100 μL of hydrofluoric acid. The solution was subsequently transferred to a Teflon-lined autoclave and sonicated for 10 min. The autoclave was then placed in an oven at 220°C for 8 h. Upon reaching room temperature, the precipitates were thoroughly washed and boiled with DMF and methanol, respectively.

Preparation of rGO

150 mg of GO was well dispersed in 50 mL of deionized water. After being sonicated,

the mixed solution was converted into a Teflon-lined autoclave. Then the autoclave was heated to 180°C and kept for 6 h. Finally, the product was collected by filtration and freeze-drying.

Preparation of rGO-MIL-101(Cr)

150 mg of GO was well dispersed in 50 mL of deionized water with 250 mg of MIL-101(Cr) powder added subsequently. After being sonicated, the mixed solution was converted into a Teflon-lined autoclave. Then the autoclave was heated to 180°C and kept for 6 h. Finally, the product rGO-MIL-101(Cr) hybrid was collected by filtration and freeze-drying.

Preparation of RM-MOF, rGO-RM-MOF and rGO-DTT

At first, 0.496 g of DTT was dissolved in the 10 mL of trichloromethane to form a homogeneous transparent solution under an Argon atmosphere. After that, 200 mg of MIL-101(Cr) (or rGO-RM-MOF) powder was activated in a vacuum at 150°C for 12 h to remove the coordinated H_2O in MOF. Before the MOF powder cooled down, the DTT solution was quickly injected. Then the mixture was stirred overnight and the RM-MOF (or rGO-RM-MOF) sample was gathered by filtration and washed several times with trichloromethane. rGO-DTT was prepared using the same method as RM-MOF, with rGO substituted for MOF.

Preparation of sulfur cathode

As for the CR2032 coin-type cell, the cathodes were prepared as below. Initially, the sublimated sulfur powder was mixed with rGO-MOFs (or rGO-DTT) in a mass ratio of 5:1. The resultant powder was encapsulated within a Teflon-lined autoclave under an argon atmosphere and then subjected to a thermal process at 155°C for 12 hours. Subsequently, the resulting yield was combined with CNTs, graphene, and PVDF in NMP, maintaining a weight ratio of 7.5:1.2:0.3:1, and stirred for 12 hours. Following this, the slurry was coated in carbon-coated aluminum foil and dried at 60°C for 12 hours. The sulfur loading of the conventional cathode typically ranged from 1.5 to 2 mg cm^{-2}. For the pouch cell and high sulfur loading (> 8 mg cm^{-2}) coin cells, KB and rGO-RM-MOF were mixed in a weight ratio of 2:5 by ball-milling for 4 h. Then sulfur powder was added and then subjected to a thermal process at 155°C to obtain S/KB-

rGO-RM-MOF. The cathode consisted of an 80 wt% blend of S/KB-rGO-RM-MOF composites, supplemented with 8 wt% acetylene black, 2 wt% graphene, and 10 wt% polyethylene oxide (PEO) in acetonitrile. This mixture was then cast onto carbon-coated aluminum foil with a shape of 4.3 × 5.6 cm^2 and subsequently dried at 60°C overnight.

Materials characterizations

The phases of samples were carried out by Powder X-ray diffraction (PXRD, SmartLabTM 9 kW X-ray diffractometer using Cu Kα radiation, λ = 1.541 Å; 2θ from 3 to 60° at 40 kV). Field-emission scanning electron microscope (FEISEM, Thermo scientific Apreo C, USA) and transmission electron microscope (TEM, Talos F200S, FEI, Thermo) were performed for the morphology of the samples. Energy-dispersive X-ray (EDX) elemental mapping measurement was carried out by TEM. The specific surface area was examined by the Brunauer Emmett Teller method using Nitrogen adsorption (Micromeritics ASAP 2460). X-ray photoelectron spectroscopy (XPS) was measured with Thermo Fisher Escalab 250Xi. Thermogravimetric analyses (TGA) were using the Perkin Elmer TGA 4000 system under a nitrogen (N_2) atmosphere to analyze the content of the materials. The Raman measurements were assembled with an *in-situ* Raman sample chamber (provided by Beijing Science Star Technology Co., Ltd. China) using a 532 nm laser source. The ultraviolet-visible (UV-vis) spectra were collected by a spectrophotometer (UV-2600). An UltiMate 3000-TSQ Endura UPLC–MS/MS system (Thermo Fisher Scientific) and a Syncronis HILIC Column (100 x 2.1 mm, 1.7 μm) at 40°C were used for chromatographic separation. The samples (MOF powders or S/MOF cathodes) were thoroughly washed and digested with concentrated HCl before the test. The gradient elution solvents were composed of acetonitrile (A) and 0.1% formic acid in water (B), and the gradient program was performed as follows: 0–2 min, 90% A; 2–5 min, 90-70% A; 5–8 min; 70–90% A; and 8.1–10 min, 90% A, flowing at 0.25 mL/min. The injection volume was 2 μL. Mass spectrometric detection was carried out using a TSQ Endura triple quadruple mass spectrometer with an electrospray ionization source. Compound-dependent parameters of the mass spectrometer were set as follows: spray voltage at 3500 V, capillary temperature at

320°C, vaporizer temperature at 350°C, sheath gas at 35 (Arb), and auxiliary gas at 10 (Arb). The detections were operated in the selective reaction monitor (SRM) positive mode with transitions of m/z 150.2 →104.1511 for Met; 385.45 → 134.111 for SAH and m/z 399.35 →250.111 for SAM, respectively. Instrument controlling and data acquiring were performed using an Xcalibur workstation (Thermo Fisher Scientific).

Electrochemical measurements

Electrochemical impedance spectroscopy (EIS) and cyclic voltammetry (CV) were conducted using CR2032 coin-type cells on an electrochemical workstation (AutoLab 302N). EIS spectra were collected from 1.0 MHz to 0.1 Hz at the cells' open circuit potential with an AC current amplitude of 10 mV. CV curves were carried out at scan rates of 0.1 to 0.5 mV s^{-1} in the voltage window of 1.7-2.8 V. The coin cells were assembled with the electrolyte composed of 1 M LiTFSI in DOL/DME (1:1 v/v) with 2 wt% $LiNO_3$ added and an electrolyte/sulfur (E/S) ratio is 3.5-18.0 μL mg^{-1}. For pouch cells, the cathode was paired with Li foil (thickness: 50-75 μm; China Energy Lithium Co., Ltd) by a battery lamination technology. The electrolyte was 1 M LiTFSI dissolved in DOL and DME (1:1 v/v) with 5 wt% $LiNO_3$. The tests of the cells were conducted using the Neware battery test system (CT-ZWJ-4'S-T-1U, Shenzhen, China) at a voltage range of 1.7-2.8 V for coin cells and 1.7-2.55 V for pouch cells. For the Galvanostatic intermittent titration technique (GITT) test, the batteries were discharged at 0.1 C (1 C = 1675 mAh g^{-1}) for 10 min followed by relaxation at the open circuit for 30 min in each step.

The ionic diffusion coefficient (D_{Li^+}) is calculated from the Randles-Sevcik equation:

$$I_{peak} = 2.69 \times 10^5 n^{1.5} A D_{Li^+}^{0.5} C_{Li^+} v^{0.5} \quad (1)$$

Where I_{peak} is the peak current (A), n is the number of electrons transferred during the reaction (n = 2 for LSB), A is the electrode area (1.13 cm^2), D_{Li^+} is the Li^+ diffusion coefficient (cm^2 s^{-1}), C_{Li^+} is the concentration of lithium-ion in the electrolyte (1 mol L^{-1}), and v is the scanning rate (V s^{-1}).

The internal reaction resistances (ΔiR) were was calculated according to Equation 2:

$$\Delta R_{internal}(\Omega) = \frac{|\Delta V_{QOCV\,-\,CCV}|}{I_{applied}} \quad (2)$$

where $^{\Delta V_{QOCV\,-\,CCV}}$ is the voltage difference between the closed voltage point (CCV) and the quasi-open circuit voltage (QOCV) point and $^{I_{applied}}$ is the applied current for the cell.

The electrochemical reactions with traditional sulfur cathode are shown in Equation 3 and 4.

Discharge: $S_8 + 16Li^+ + 16e^- \rightarrow 8Li_2S$ (3)

Charge: $8Li_2S \rightarrow S_8 + 16Li^+ + 16e^-$ (4)

And the electrochemical reactions of S/RM-MOF cathode are shown in Equation 5-7.

Discharge (First cycle): $S_8 + 16Li^+ + 16e^- \rightarrow 8Li_2S$ (5)

Charge:

$2RM - MOF - DTT - Li + 8Li_2S \rightarrow 2RM - MOF - DTT - S_4Li + 16Li^+ + 16e^-$

(6)

Discharge: $2RM - MOF - DTT - S_4Li + 16Li^+ + 16e^- \rightarrow 8Li_2S + 2RM - MOF - DTT - Li$ (7)

Visualized Li_2S_6 adsorption test

A 0.02 M Li_2S_6 solution was synthesized by dissolving sulfur and Li_2S in a 5:1 molar ratio in a 1 M LiTFSI solution in a 1:1 volume ratio of DOL/DME with 2 wt% $LiNO_3$ added as an electrolyte. The solution was stirred vigorously at 80°C for 18 h to ensure complete dissolution. Then, 20 mg of samples were added to 5 mL of the above as-prepared Li_2S_6 solutions. After standing for 12 h, the samples were diluted 50 times and subjected to UV-vis absorption spectra to further compare with the concentration of Li_2S_6. All the above operations were carried out in an argon-filled glove box.

Symmetrical cell assembly and corresponding electrochemical test

Li_2S_6 electrolyte (0.2 M) was prepared by the same method as the one mentioned above.

The electrode was fabricated by blending rGO, rGO-RM-MOF, and rGO-MIL-101(Cr) with PVDF in a weight ratio of 9:1 within the NMP solvent. Subsequently, the resultant slurry was uniformly coated onto an aluminum foil substrate to achieve a mass loading of 1 mg cm^{-2}. The cells were assembled with two identical electrodes and a PP separator with 15 μL of as-prepared Li_2S_6 electrolyte added. The CV measurements of the symmetric cells were performed with a voltage window between –1.0 to 1.0 V at a scan rate of 50 mV s^{-1}. The EIS was performed in a frequency range of 0.1 to 10^5 Hz.

Li_2S nucleation measurements

The 0.2 M Li_2S_8 electrolyte was synthesized by combining Li_2S and elemental sulfur in a solvent of tetraethylene glycol dimethyl ether, maintaining a molar ratio of 1:7, and the mixture was subjected to vigorous stirring at a temperature of 80°C for 12 h. Two identical electrodes were prepared in a symmetrical cell assembly test and a PP separator was used to assemble the cells. 25 μL of Li_2S_8 electrolyte was dropped onto the cathode, and 20 μL of conventional electrolyte was added to the anode side. Then the cell was subjected to galvanostatic discharge under a current density of 112 μA until reaching 2.06 V and kept potentiostatically at 2.05 V for Li_2S to nucleate until the current dropped below 10^{-5} A.

Density functional theory (DFT) calculation

First-principles calculations were carried out by the Vienna *ab initio* simulation package (VASP). The projector augmented wave (PAW). Pseudopotentials were used for describing the interaction among electrons and nuclei, with an energy cutoff of 500 eV for the plane wave basis. The generalized gradient approximation (GGA) exchange-correlation energy was profiled by the Perdew-Burke-Ernzerhof (PBE). The criteria of the total energy convergence were set to 10^{-4} eV and all structures were relaxed to a force tolerance of less than 0.05 eV/Å. Gamma-center grids were adopted to sample the Brillouin zone, with 1×1×1 k-mesh. The vdW-DF3 functional was applied to describe the van der Waals (vdW) interactions in the LSB systems. The Bader charge analysis was used to study the charge transfer mechanism between Li_2S_6 and different MOFs. The adsorption energies (E_{ads}) were calculated as follows

$$E_{ads} = E_{Li_2S_x/sub} - E_{Li_2S_x} - E_{sub}$$

Where $E_{Li_2S_x/sub}$, $E_{Li_2S_x}$ and E_{sub} are the total energies of the optimized adsorbate/substrate system, the Li_2S_x (S_8, Li_2S_8, Li_2S_6, Li_2S_4, Li_2S_2, and Li_2S) in the structure, and the clean substrate, respectively.

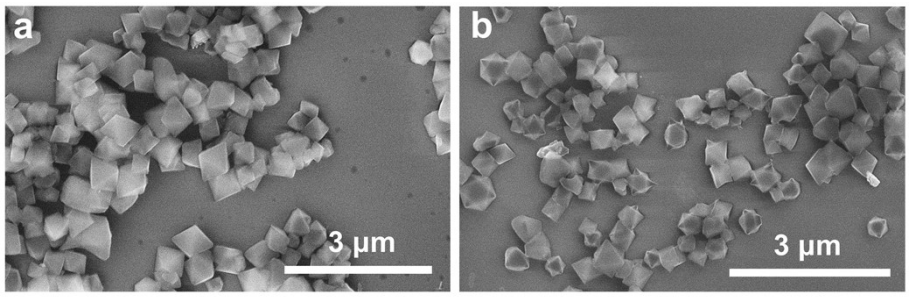

Fig. S1. SEM images of (a) MIL-101(Cr) and (b) RM-MOF.

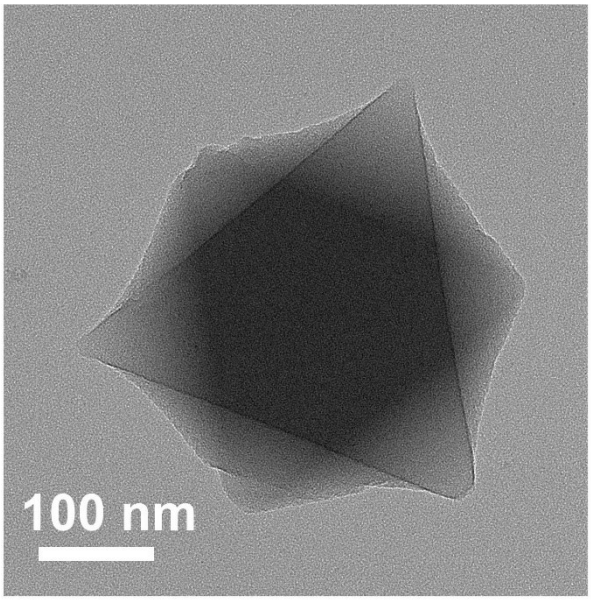

Fig. S2. TEM image of RM-MOF.

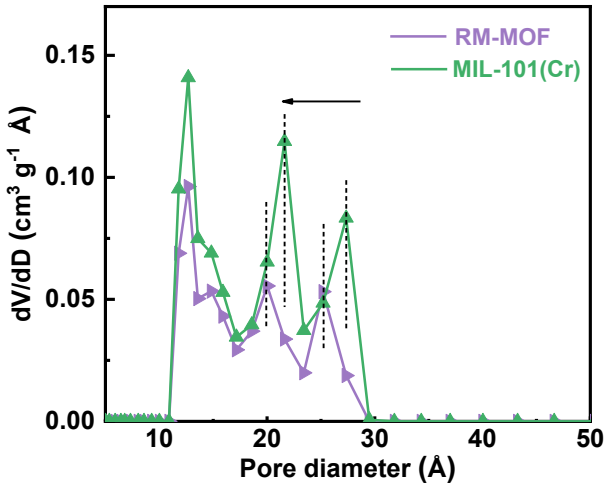

Fig. S3. Pore size distribution of MIL-101(Cr) and RM-MOF.

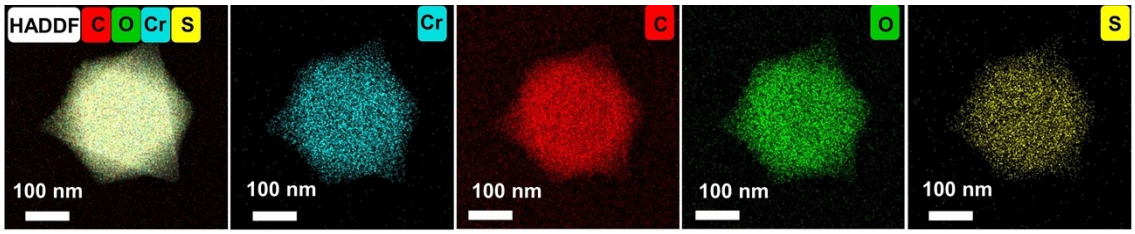

Fig. S4. EDS mapping images of RM-MOF.

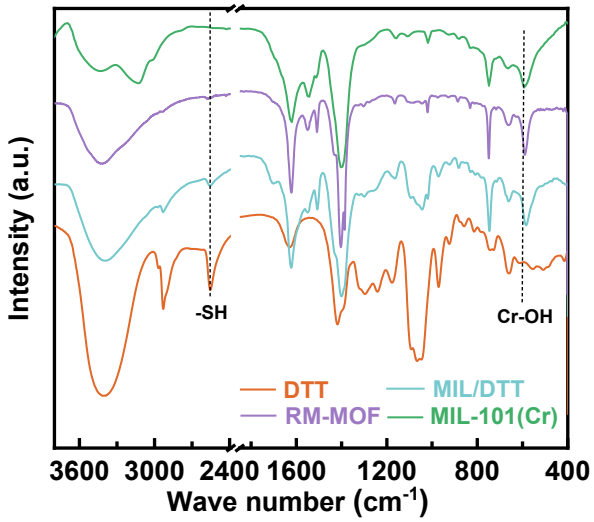

Fig. S5. FT-IR spectra of MIL-101(Cr), DTT, MIL/DTT, and RM-MOF.

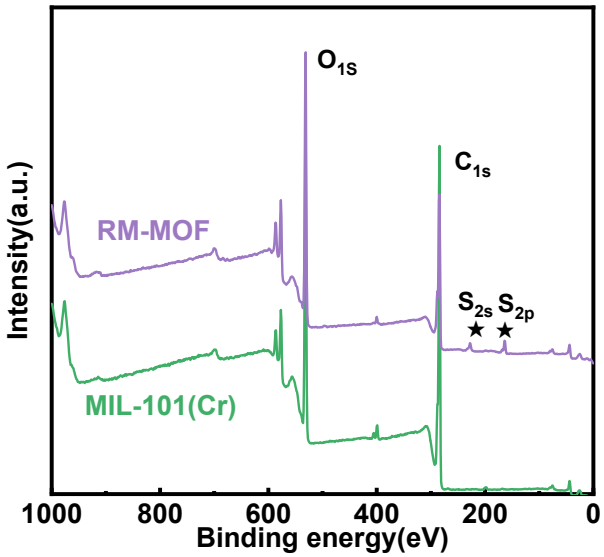

Fig. S6. XPS survey spectra of MIL-101(Cr) and RM-MOF.

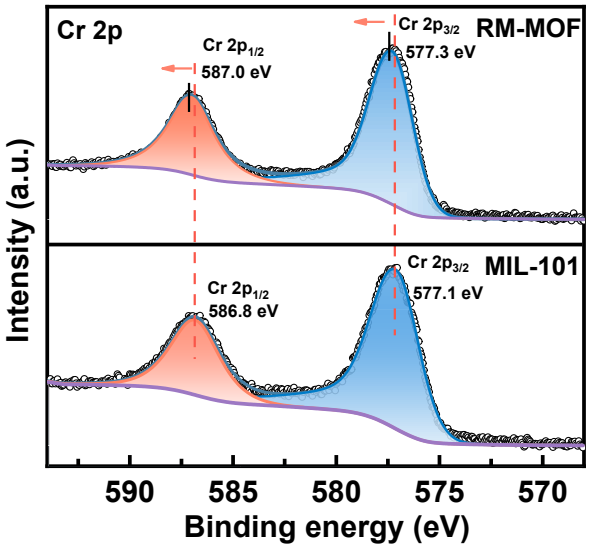

Fig. S7. High-resolution XPS spectra of Cr 2p of MIL-101(Cr) and RM-MOF.

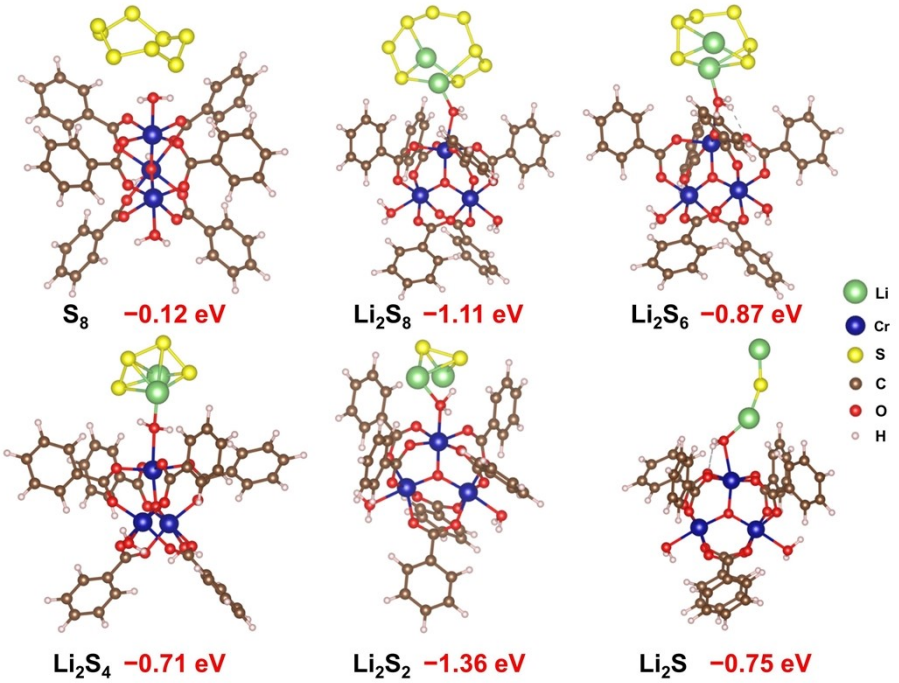

Fig. S8. DFT calculation of the optimized adsorption configuration and energies between MIL-101(Cr) and Li_2S_n (n =0, 2, 4, 6, and 8).

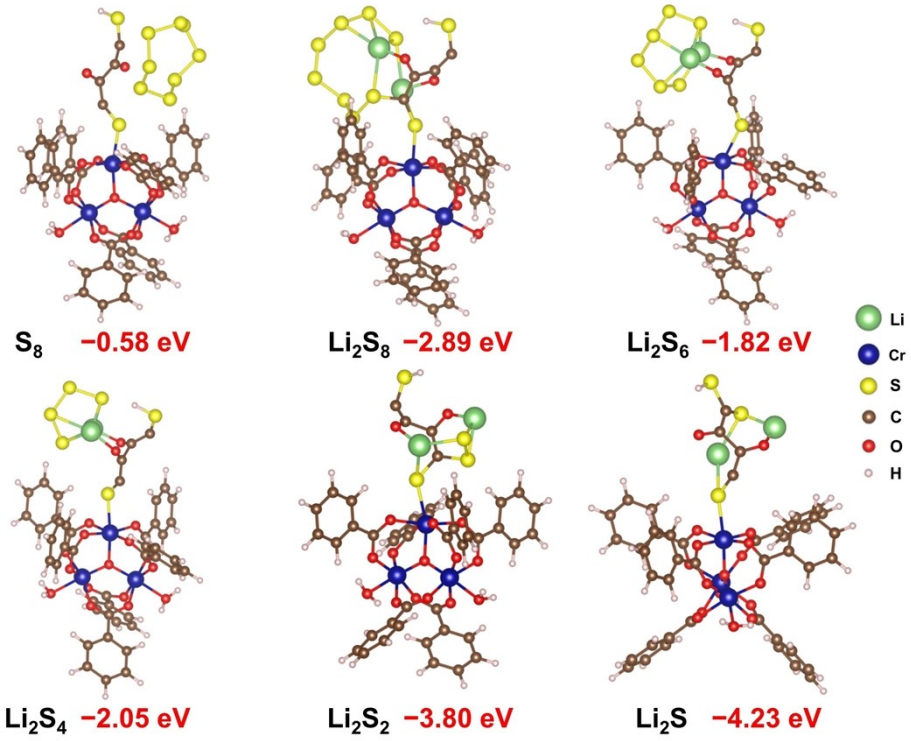

Fig. S9. DFT calculation of the optimized adsorption configuration and energies between RM-MOF and Li_2S_n (n =0, 2, 4, 6, and 8).

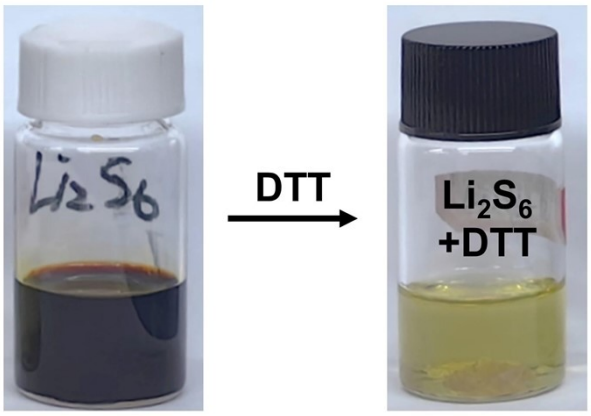

Fig. S10. Optical diagram of the color change of 0.2 M Li_2S_6 solution after reaction with DTT.

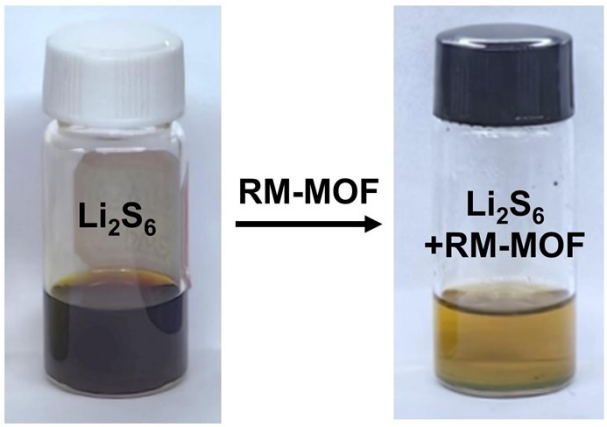

Fig. S11. Optical diagram of the color change of 0.2 M Li_2S_6 solution after reaction with RM-MOF.

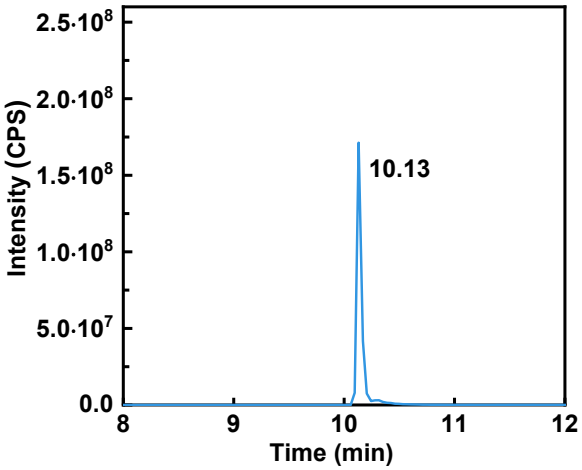

Fig. S12. Total ion chromatogram of the RM-MOF reacted with LiPSs.

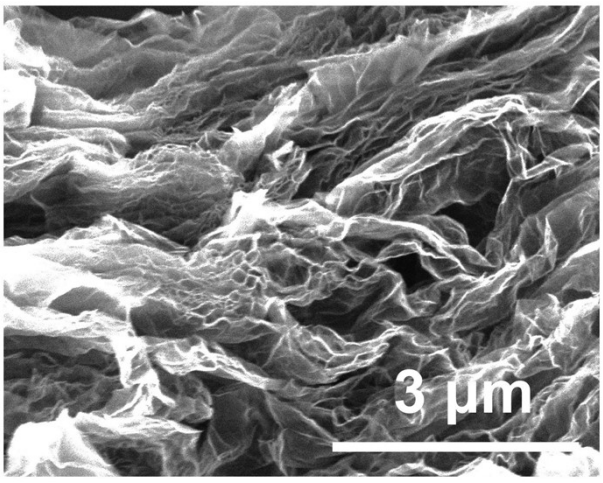

Fig. S13. SEM image of rGO.

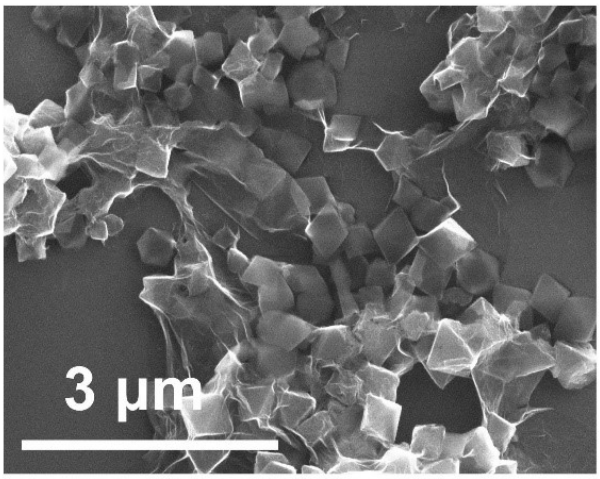

Fig. S14. SEM image of rGO-RM-MOF.

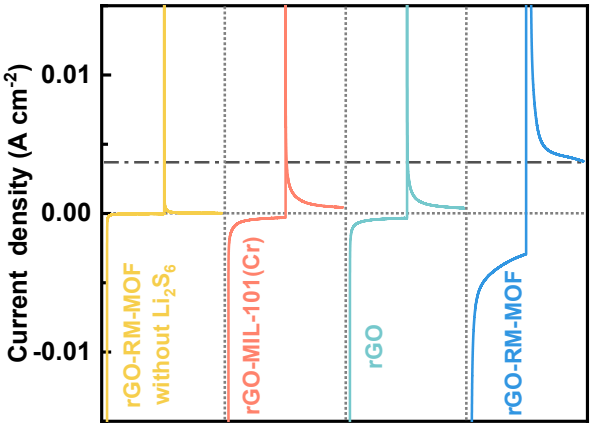

Fig. S15. Chronoamperometry curves of symmetric cells with rGO-MIL-101(Cr), rGO, rGO-RM-MOF as electrodes and Li_2S_6 solution as electrolytes.

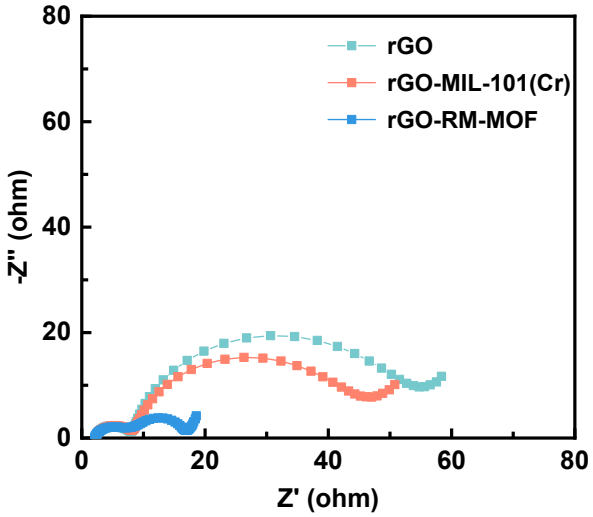

Fig. S16. EIS curves of Li_2S_6 symmetric cells with rGO-MIL-101(Cr), rGO, and rGO-RM-MOF as electrodes.

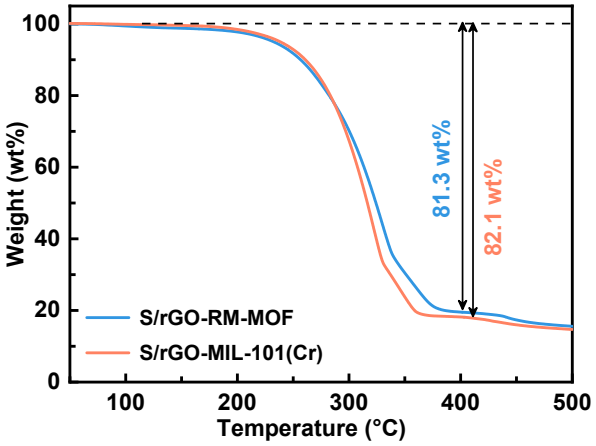

Fig. S17. TGA curves of S/rGO-MIL-101(Cr) and S/rGO-RM-MOF.

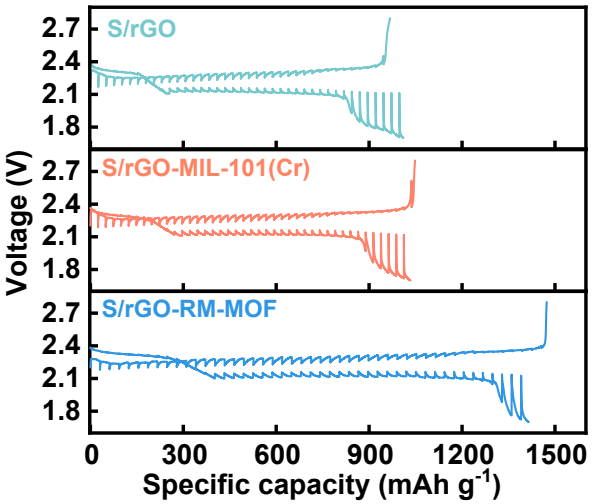

Fig. S18. The GITT plots of lithium−sulfur batteries (LSBs) with different cathodes at 0.1 C.

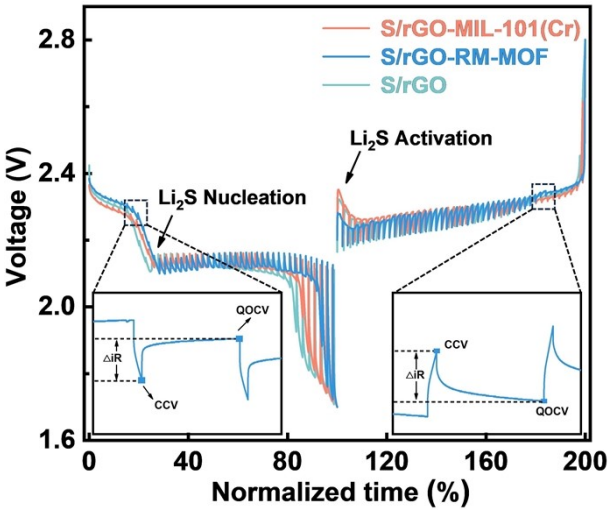

Fig. S19. The GITT plots of LSBs with different cathodes under normalized time.

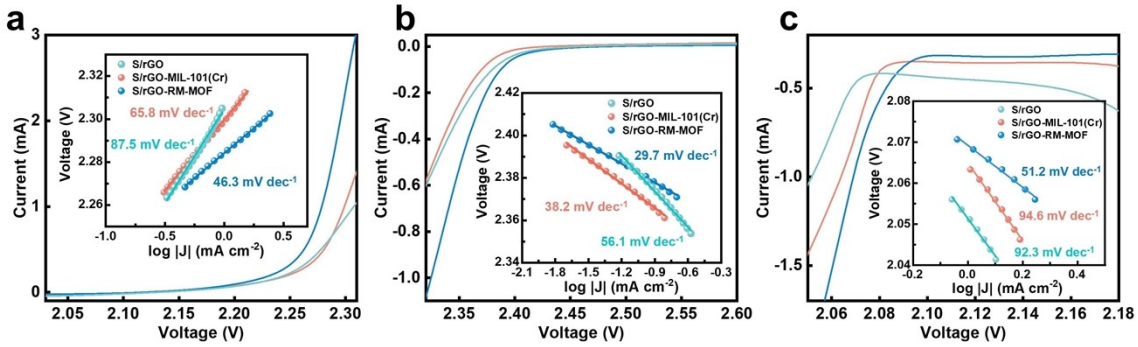

Fig. S20. CV curves of the LSBs with S/rGO-MIL-101(Cr), S/rGO, and S/rGO-RM-MOF cathodes over different voltage windows. The insets are the corresponding Tafel plots corresponding to (a) peak A, (b) peak B, and (c) peak C.

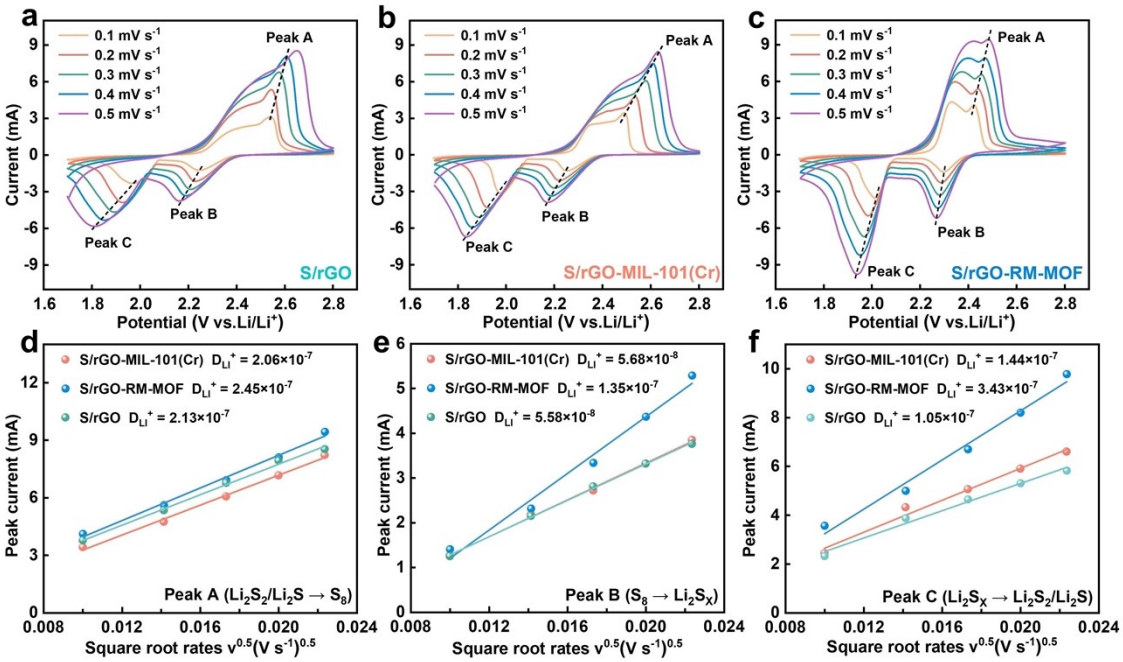

Fig. S21. CV curves of LSBs paired with different cathodes: (a) S/rGO, (b) S/rGO-MIL-101(Cr), and (c) S/rGO-RM-MOF at different scan rates from 0.1 to 0.5 mV s^{-1}. Plots of CV peak current of (d) anodic oxidation process (peak A), (e) first cathodic reduction process (peak B), and (f) second cathodic reduction process (peak C) vs square root of the scan rate.

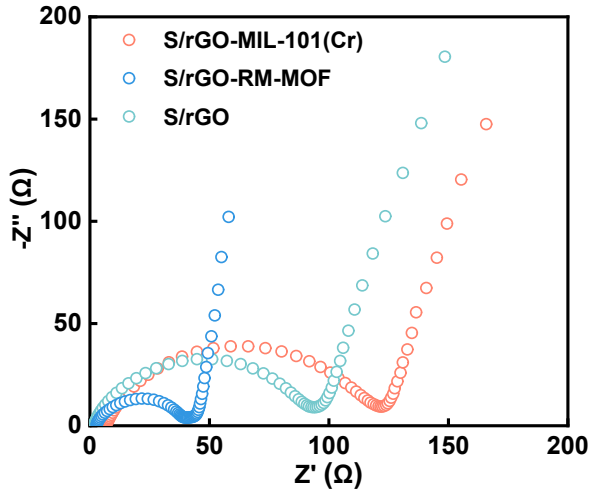

Fig. S22. EIS curves of the LSBs with different cathodes at open circuit voltage (OCV).

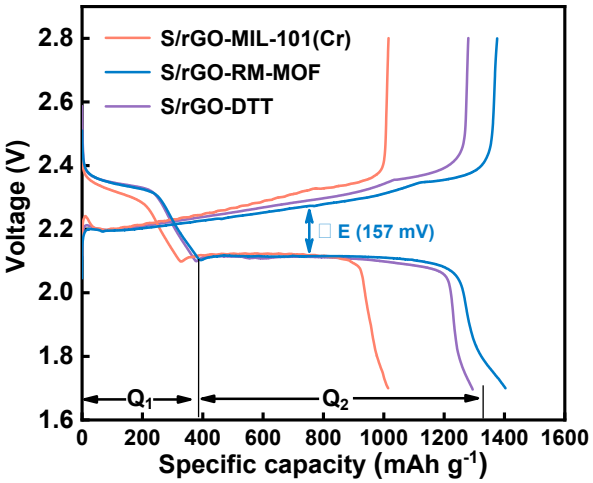

Fig. S23. Charge/discharge profiles of the LSBs with different cathodes.

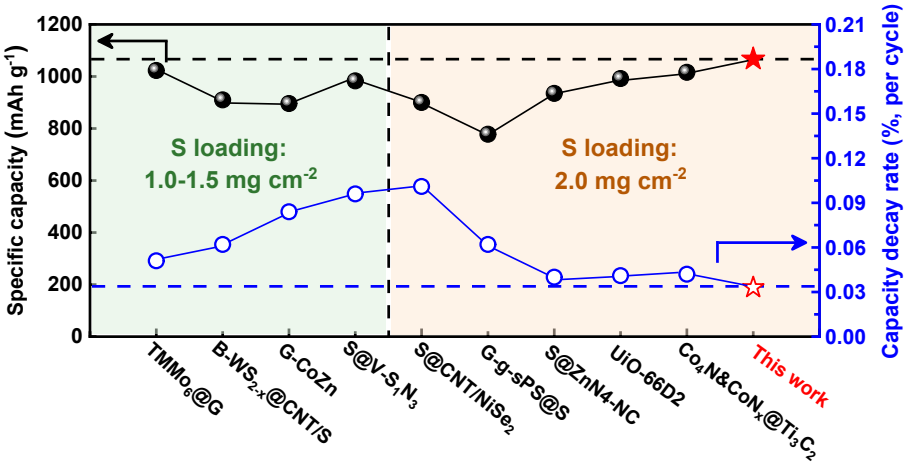

Fig. S24. Comparison of electrochemical performance of LSBs with different catalytic materials or mediators at 1 C.

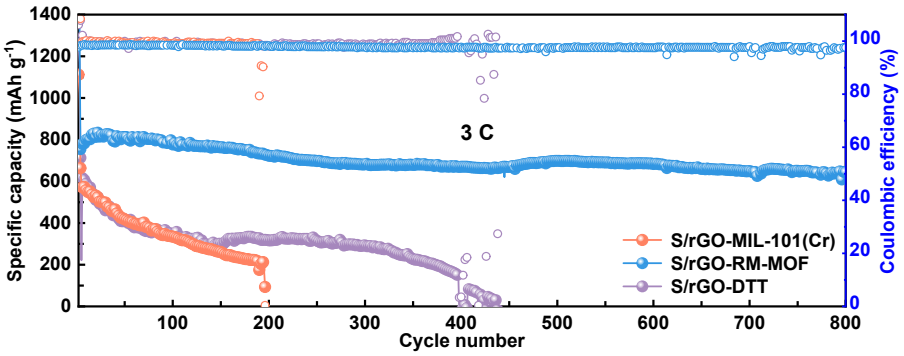

Fig. S25. Cycling performance of LSBs with different cathodes at 3 C.

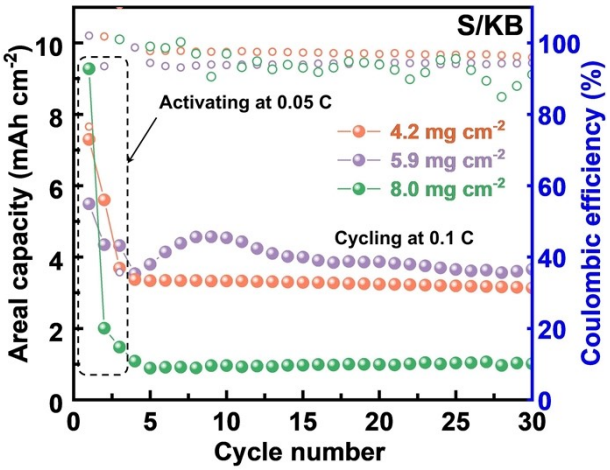

Fig. S26. Cycling stability of LSBs with S/KB cathode under high sulfur loadings at 0.1 C.

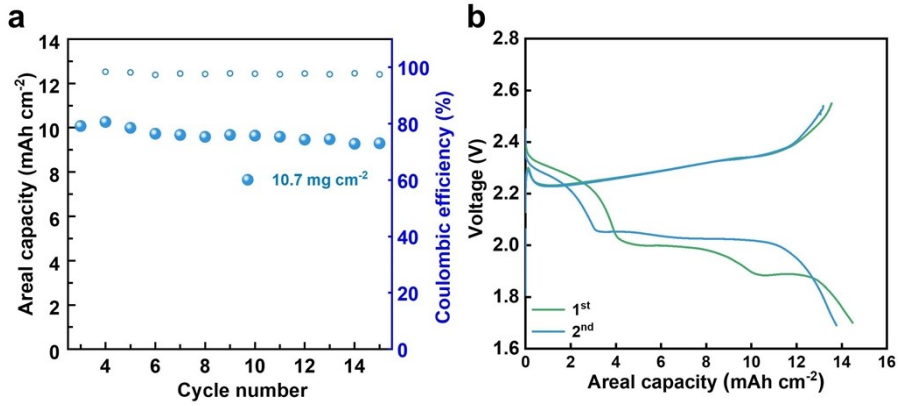

Fig. S27. (a) Cycling performance of LSBs with S/rGO-RM-MOF under sulfur loadings of 10.7 mg cm^{-2} at 0.1 C. (b) Charge/discharge profiles of LSBs with S/rGO-RM-MOF under sulfur loadings of 15.4 mg cm^{-2} at 0.05 C.

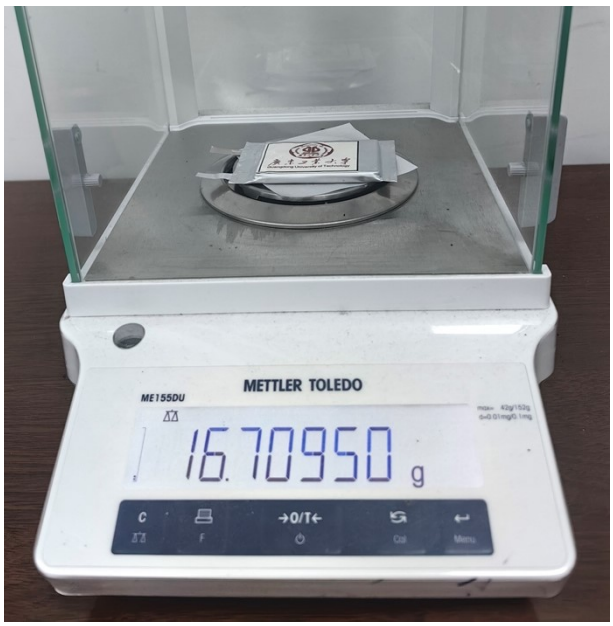

Fig. S28. The total weight of the 2.6 Ah-level Li-S pouch cell.

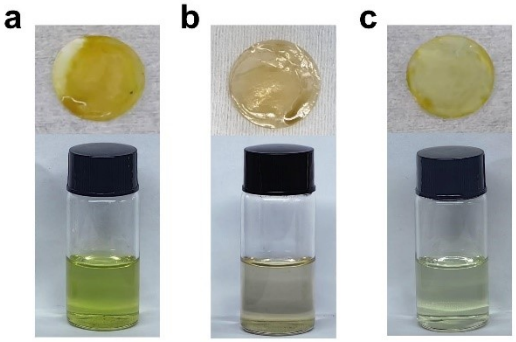

Fig. S29. Digital images of the separators and leacheate obtained from the LSBs with (a) S/rGO-MIL-101(Cr), (b) S/rGO-DTT, and (c) S/rGO-RM-MOF after cycling. The leacheate was obtained by immersing the disassembled LSBs in a 10 mL solution of 1,3-dioxolane (DOL)/1,2-dimethoxymethane (DME) (1:1, v/v) to wash out the generated LiPSs.

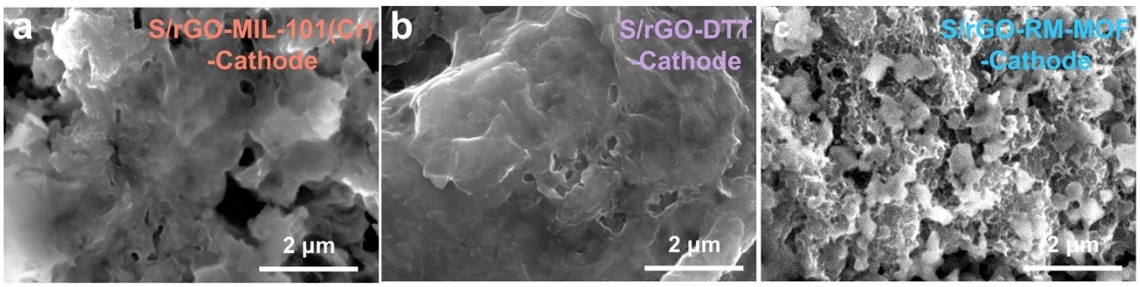

Fig. S30. Surface morphologies of cathodes after cycling for LSBs with (a) S/rGO-MIL-101(Cr), (b) S/rGO-DTT, and (c) S/rGO-RM-MOF.

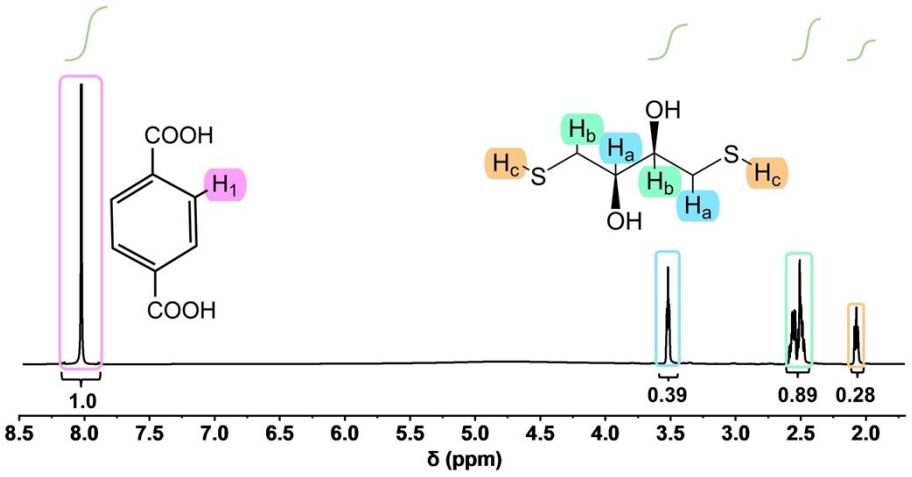

Fig. S31. ^{1}H NMR spectrum of the digested RM-MOF in DMSO-d_6. Accordingly, the structural formula of RM-MOF is calculated to be $[Cr_3OF(bdc)_3(H_2O)_{0.32}DTT_{1.68}]_n$.

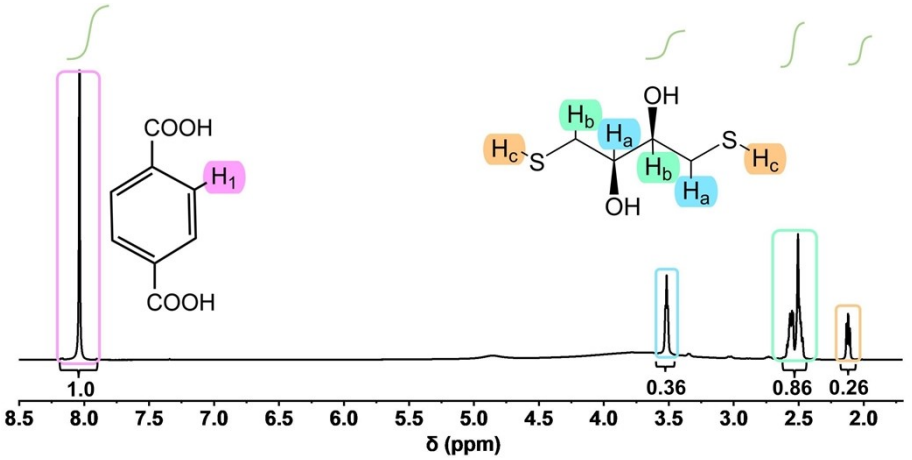

Fig. S32. ^{1}H NMR spectrum of digested RM-MOF for the LSBs after 100 cycles in DMSO-d_6.

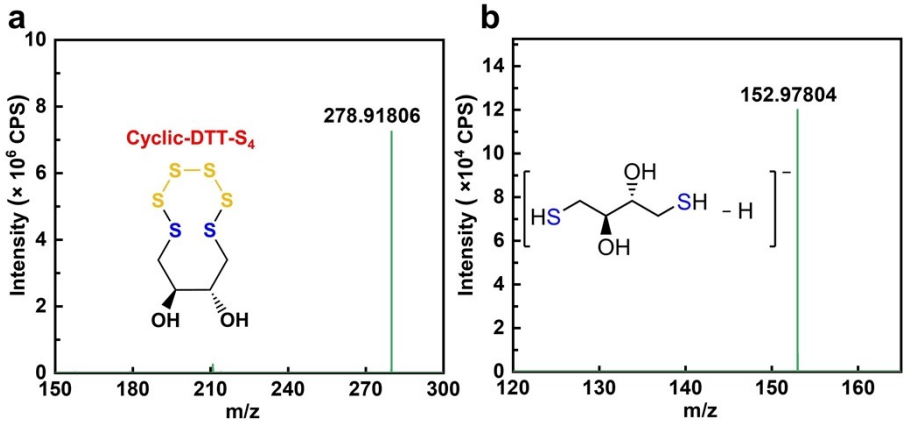

Fig. S33. (a) Mass spectrum of S/rGO-DTT cathode after recharging. (b) Mass spectrum of the discharged product of the LSBs with S/rGO-DTT.

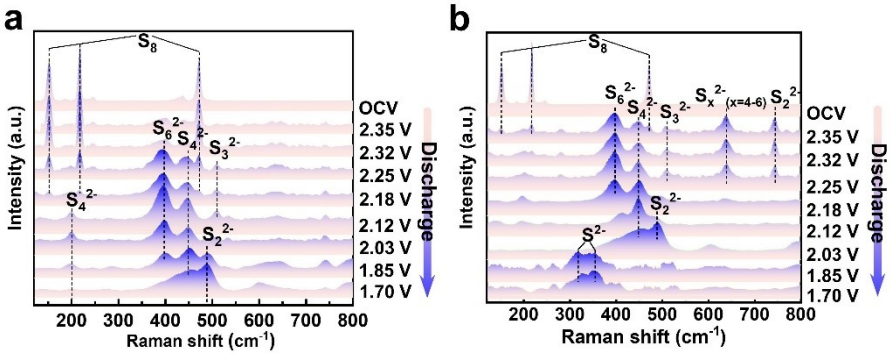

Fig. S34. *In situ* voltage-resolved Raman spectra of the discharge process of the cathode side in the LSBs with (a) S/rGO-MIL-101(Cr) cathode and (b) S/rGO-RM-MOF cathode.

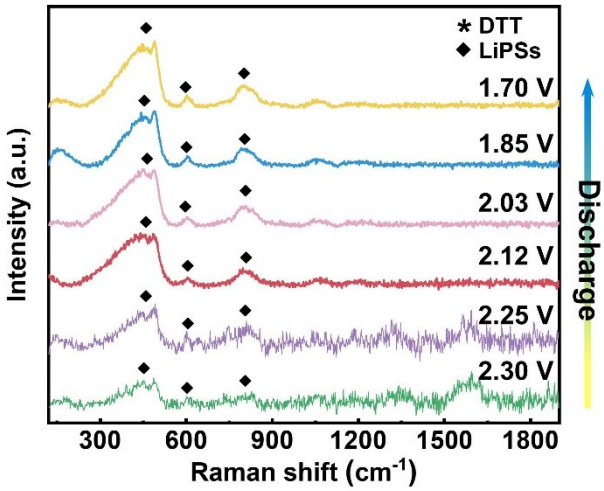

Fig. S35. Raman spectra of the discharge process of the anode side in the LSBs with S/rGO-MIL-101(Cr). The PP separator near the anode side was exposed to the incident laser beam.

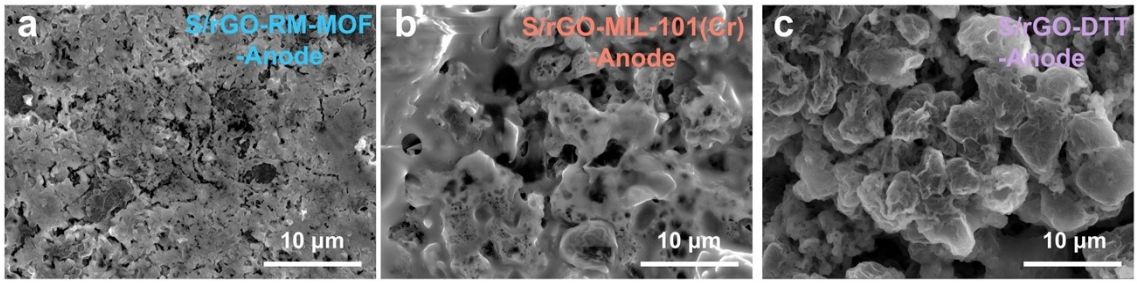

Fig. S36. Surface morphologies of lithium plates after cycling disassembled from LSBs with (a) S/rGO-RM-MOF, (b) S/rGO-MIL-101(Cr), and (c) S/rGO-DTT.

Table S1. Lithium-ion diffusion coefficient (D_{Li^+}, $cm^2\ s^{-1}$) of LSBs paired with different cathodes.

Samples	Peak A	Peak B	Peak C
S/rGO-MIL-101(Cr)	2.06×10^{-7}	5.68×10^{-8}	1.44×10^{-7}
S/rGO	2.13×10^{-7}	5.58×10^{-8}	1.05×10^{-7}
S/rGO-RM-MOF	2.45×10^{-7}	1.35×10^{-7}	3.43×10^{-7}

Table S2. Electrode polarization voltage (ΔE) values of LSBs with different cathodes.

Samples	ΔE (mV)
S/rGO-MIL-101(Cr)	205
S/rGO-DTT	180
S/rGO-RM-MOF	157

Table S3. Q_2/Q_1 ratio of LSBs with different cathodes.

Samples	Q_1 (mAh g^{-1})	Q_2 (mAh g^{-1})	Q_2/Q_1
S/rGO-MIL-101(Cr)	330.32	683.11	2.06
S/rGO-DTT	378.62	916.05	2.42
S/rGO-RM-MOF	385.20	1018.03	2.64

Table S4. Comparison of electrochemical performance of LSBs with different catalytic sulfur hosts previously reported.

Component	S mass loading (mg cm^{-2})	Specific capacity (mAh g^{-1})	Capacity decay rate (%, per cycle)	Ref.
S/rGO-RM-MOF	2.0	1067 (1 C) 830 (3 C)	0.038 (1000 cycles, 1 C) 0.033 (800 cycles, 3 C)	This work
Co_4N&CoN_x@Ti_3C_2	2.0	1,016 (1 C)	0.042 (1000 cycles, 1 C)	[1]
UiO-66D2	2.0	992 (1 C)	0.041 (500 cycles, 1 C)	[2]

S@ZnN_4-NC	2.0	935 (1 C) 787 (2 C)	0.040 (500 cycles, 1 C)	3
G-g-sPS@S	2.0	778 (1 C)	0.062 (200 cycles, 1 C)	4
S@CNT/$NiSe_2$	2.0	900 (1 C)	0.101 (500 cycles, 1 C)	5
S@V-S_1N_3	1.0	983 (1 C)	0.076 (600 cycles, 1 C)	6
G-CoZn	1.0	896 (1 C) 784 (2 C)	0.084 (300 cycles, 1 C) 0.042 (1000 cycles, 2 C)	7
B−WS_{2-x}@CNT/S	1.5	910 (1 C) 760 (3 C)	0.062 (500 cycles, 1 C) 0.080 (500 cycles, 3 C)	8
$TMMo_6$@G	1.5	1023 (1 C)	0.051 (750 cycles, 1 C)	9
D-ZIF-L	1.5	820 (1 C)	0.058 (500 cycles, 1 C)	10
w-PBDT	1.0	1011 (0.5 C) 907 (2 C)	0.088 (500 cycles, 0.5 C) 0.126 (280 cycles, 2 C)	11
ZnCo-MOF/S	1.6	806 (0.5 C) 676 (1 C)	0.048 (300 cycles, 0.5 C)	12
S@CoNiMOF	1.5	993 (0.2 C)	0.076 (400 cycles, 0.2 C)	13
SAIn@CNT	1.5	1306 (0.5 C) 1100 (1 C)	0.093 (500 cycles, 0.5 C)	14

Table S5. Comparison of electrochemical performance of LSBs under high sulfur loadings assembled with different MOF-based sulfur hosts as well as redox mediators previously reported.

Component	**S mass loading (mg cm^{-2})**	**E/S ratio (μL mg^{-1})**	**specific capacity (mAh g^{-1})**	**Energy density (Wh kg^{-1})**	**Ref.**
S@CoNiMOF	4.6	-	900(1 C)	28.3	13
S@Ni-MOF-1D	4.3	12	1244(0.1 C)		
	5.5	9.4	1064(0.1 C)	-	15
	6.7	7.6	992(0.1 C)		
S/Quasi-MOF NS	3.5	8.6	914(0.5 C)	-	16
	5	6	800(0.5 C)		
	6.5	4.6	707.7(0.5 C)		
S/ZIF-7 600	5.1	5.2	901.9(0.1 C)	20.1	17
	7.6	3.8	684.2(0.1 C)		
G-g-sPS@S	5.5		818.2(0.1 C)		
	7.8	-	743.6(0.1 C)	-	4
	10.5		1019.0(0.1 C)		

THPP	4.9	-	816.3(0.1 C)	-	[18]
ppy-por	5 4	6.8 7	900(0.2 C) 725(0.05 C)	-	[19]
w-PBDT	3.8	3.5	1413 (0.05 C)	290	[11]
S@V-S_1N_3	3.5 4.2		742.8(0.1 C) 761.9(0.1 C)	-	[6]
DIPS-EPSE	6.1	2.7	843 (0.05)	217	[20]
VC@INFeD	4 4.5 5.2	7 7 7	725(0.05 C) 515.5(0.05 C) 440.4(0.05 C)	-	[21]
UiO-66-D2	3.5	-	-	40.2	[2]
TO/DME	7.6	3.5	1175(0.025)	304	[22]
S/D-ZIF L	5	3	703(0.05 C)	254	[10]
S-CF_X	6.4	2.5	1371(0.05 C)	81	[23]
Li_xMoS_2	2.5 5 7.5 10	12	1275 1200 1100 800	184	[24]
S@CNT/$NiSe_2$	3.6 5.7 8.2	8	1028(0.05 C) 905(0.05 C) 1005(0.05 C)	-	[5]
CoZn/Carbon	5 10	4.8	1170 (0.2 C) 800 (0.2 C)	-	[25]
S/rGO-RM-MOF	4.1 6.3 7.8 10.7 15.4	10 7.9 5.8 4.6 3.5	1219.5(0.1 C) 1063.5(0.1 C) 1012.8(0.1 C) 943.9(0.1 C) 896.1(0.05 C)	316.5	This work

The energy density was calculated as follows based on the total mass of the pouch cell:

$$Energy\ density = \frac{M_{sulfur} * Voltage * Specific\ capcity}{M_{total}}$$

The unaccounted mass of sulfur in the corresponding references was calculated according to specified cathode parameters. The unaccounted average voltage was

directly obtained from the graph. The total mass of the pouch cell was estimated by the parameters of pouch cells in articles.

Table S6. Relevant parameters of the high-energy density Ah-level pouch cell.

Parameters	value
Number of cathodes	9
Sulfur mass (g)	2.03
E/S ratio (electrolyte gs^{-1})	2.91
Specific capacity (mAh g^{-1})	1271
Discharge capacity (Ah)	2.58
Total weight of pouch cell (g)	16.71
Energy density (Wh kg^{-1})	316.53

Reference

1. T. Wang, Q. Dong, F. Wang, R. Xu, C. Tong, D. Su, M. Shao, C. Li and Z. Wei, *Matter*, 2024, **7**, 1035-1053.
2. X. Wang, X. Zhang, Y. Zhao, D. Luo, L. Shui, Y. Li, G. Ma, Y. Zhu, Y. Zhang, G. Zhou, A. Yu and Z. Chen, *Angew. Chem. Int. Ed.*, 2023, **62**, e202306901.
3. X. Zhang, T. Yang, Y. Zhang, X. Wang, J. Wang, Y. Li, A. Yu, X. Wang and Z. Chen, *Adv. Mater.*, 2023, **35**, 2208470.
4. J. Wu, J. Huang, Y. Cui, D. Miao, X. Ke, Y. Lu and D. Wu, *Adv. Mater.*, 2023, **35**, 2211471.
5. Z. Han, R. Gao, T. Wang, S. Tao, Y. Jia, Z. Lao, M. Zhang, J. Zhou, C. Li, Z. Piao, X. Zhang and G. Zhou, *Nat. Catal.*, 2023, **6**, 1073-1086.
6. R. Yan, Z. Zhao, R. Zhu, M. Wu, X. Liu, M. Adeli, B. Yin, C. Cheng and S. Li, *Angew. Chem. Int. Ed.*, 2024, **63**, e202404019.
7. C. Geng, X. Jiang, S. Hong, L. Wang, Y. Zhao, J. Qi, J. Shi, J. Wang, L. Peng, Z. Hu, Y. Guo, F. Jin, Q. Yang and W. Lv, *Adv. Mater.*, 2024, **36**, 2407741.
8. Z. Lao, Z. Han, J. Ma, M. Zhang, X. Wu, Y. Jia, R. Gao, Y. Zhu, X. Xiao, K. Yu and G. Zhou, *Adv. Mater.*, 2024, **36**, 2309024.
9. Y. Li, K. Sun, Y. Fu, S. Wang, C. Zhuge, X. Yin, Z. Yang, Z. Li, D. Liu, X. Wang and D. He, *Adv. Mater.*, 2024, **36**, 2406343.
10. J. Wang, X. Zhang, X. Wang, J. Liu, S. Li, Y. Nie, K. Zong, X. Zhang, H. Meng, M. Jin, L. Yang, X. Wang and Z. Chen, *Adv. Energy Mater.*, 2024, DOI: 10.1002/aenm.202402072.
11. X. Miao, C. Song, W. Hu, Y. Ren, Y. Shen and C. Nan, *Adv. Mater.*, 2024, **36**, 2401473.
12. Z. Zhu, Y. Zeng, Z. Pei, D. Luan, X. Wang and X. W. Lou, *Angew. Chem. Int. Ed.*, 2023, **62**, e202305828
13. X. Ren, Q. Wang, Y. Pu, Q. Sun, W. Sun and L. Lu, *Adv. Mater.*, 2023, **35**, 2304120.
14. Y. Guo, Z. Jin, J. Lu, L. Wei, W. Wang, Y. Huang and A. Wang, *Energy Environ. Sci.*, 2023, **16**, 5274-5283.
15. D. Yang, Z. Liang, P. Tang, C. Zhang, M. Tang, Q. Li, J. Biendicho, J. Li, M. Heggen, R. Dunin-Borkowski, M. Xu, J. Llorca, J. Arbiol, J. Morante, S. Chou and A. Cabot, *Adv. Mater.*, 2022, **34**, 2108835.
16. D. Luo, C. Li, Y. Zhang, Q. Ma, C. Ma, Y. Nie, M. Li, X. Weng, R. Huang, Y. Zhao, L. Shui, X. Wang and Z. Chen, *Adv. Mater.*, 2022, **34**, 2105541.
17. X. Wang, C. Zhao, B. Liu, S. Zhao, Y. Zhang, L. Qian, Z. Chen, J. Wang, X. Wang and Z. Chen, *Adv. Energy Mater.*, 2022, **12**, 2201960.
18. B. Yang, D. Guo, P. Lin, L. Zhou, J. Li, G. Fang, J. Wang, H. Jin, X. Chen and S. Wang, *Angew. Chem. Int. Ed.*, 2022, **61**, e202204327.
19. C. Zhao, X. Li, M. Zhao, Z. Chen, Y. Song, W. Chen, J. Liu, B. Wang, X. Zhang, C. Chen, B. Li, J. Huang and Q. Zhang, *J. Am. Chem. Soc.*, 2021, **143**, 19865-19872.

20. L. Hou, X. Zhang, N. Yao, X. Chen, B. Li, P. Shi, C. Jin, J. Huang and Q. Zhang, *Chem*, 2022, **8**, 1083-1098.
21. T. Li, D. Cai, S. Yang, Y. Dong, S. Yu, C. Liang, X. Zhou, Y. Ge, K. Xiao, H. Nie and Z. Yang, *Adv. Mater.*, 2022, **34**, 2207074.
22. L. Hou, Y. Li, Z. Li, Q. Zhang, B. Li, C. Bi, Z. Chen, L. Su, J. Huang, R. Wen, X. Zhang and Q. Zhang, *Angew. Chem. Int. Ed.*, 2023, **62**, e202305466.
23. J. Feng, T. Liu, H. Li, Y. S. Hu, H. Mao and L. Suo, *J. Am. Chem. Soc.*, 2024, **146**, 3755-3763.
24. Z. Li, I. Sami, J. Yang, J. Li, R. V. Kumar and M. Chhowalla, *Nat. Energy*, 2023, **8**, 84-93.
25. H. Li, R. Meng, C. Ye, A. Tadich, W. Hua, Q. Gu, B. Johannessen, X. Chen, K. Davey and S.-Z. Qiao, *Nat. Nanotechnol.*, 2024, **19**, 792-799.